J. Fluid Mech. (2015), *vol.* 775, *pp.* 288–303.
doi:10.1017/jfm.2015.293

Viscous–poroelastic interaction as mechanism to create adhesion in frogs' toe pads

A. Tulchinsky[1] **and A. D. Gat**[1],†

[1]Faculty of Mechanical Engineering, Technion, Israel Institute of Technology, Haifa 32000, Israel

(Received 1 October 2014; revised 28 January 2015; accepted 19 May 2015)

The toe pads of frogs consist of soft hexagonal structures and a viscous liquid contained between and within the hexagonal structures. It has been hypothesized that this configuration creates adhesion by allowing for long-range capillary forces, or, alternatively, by allowing for exit of the liquid and thus improving contact of the toe pad. In this work, we suggest interaction between viscosity and elasticity as a mechanism to create temporary adhesion, even in the absence of capillary effects or van der Waals forces. We initially illustrate this concept experimentally by a simplified configuration consisting of two surfaces connected by a liquid bridge and elastic springs. We then utilize poroelastic mixture theory and model frogs' toe pads as an elastic porous medium, immersed within a viscous liquid and pressed against a rigid rough surface. The flow between the surface and the toe pad is modelled by the lubrication approximation. Inertia is neglected and analysis of the elastic–viscous dynamics yields a governing partial differential equation describing the flow and stress within the porous medium. Several solutions of the governing equation are presented and show a temporary adhesion due to stress created at the contact surface between the solids. This work thus may explain how some frogs (such as the torrent frog) maintain adhesion underwater and the reason for the periodic repositioning of frogs' toe pads during adhesion to surfaces.

Key words: biological fluid dynamics, low-Reynolds-number flows, porous media

1. Introduction

The toe pads of frogs consist of soft thin hexagonal structures and a viscous fluid between and within the soft structures (Ernst 1973*a*,*b*; Green 1979). It has been hypothesized that such a configuration enables attachment to surfaces by capillary forces (Emerson & Diehl 1980; Hanna, Jon & Barnes 1991; Federle 2006), or alternatively that the channel network allows for exit of the viscous liquid and thus improves contact of the toe pad with the surface (Federle *et al.* 2006; Persson 2007; Tsipenyuk & Varenberg 2014). Analytical works include Federle *et al.* (2006), who modelled the contribution of capillary forces to shear stress on the surface, and Persson (2007), who studied the effect of elasticity on capillary forces.

In this work, we suggest a mechanism for creating temporary adhesion based on the interaction between viscous flow and elastic deformation. We model the toe pads

† Email address for correspondence: amirgat@technion.ac.il

of frogs as an elastic porous medium (similarly to Battiato, Bandaru & Tartakovsky 2010 and Battiato 2012), immersed within a viscous liquid, and pressed against a solid surface with known roughness. The dynamics of the elastic porous material are studied via the poroelastic theory (Biot 1972; Bowen 1980; Ambrosi & Preziosi 2000). The flow between the frogs' toe pads and the solid surface is modelled by the lubrication approximation. Forces and kinematic constraints acting on the liquid-saturated toe pad deform the material. The deformation of the porous material creates a viscous flow within the toe pads while modifying its stress field. The viscous fluid, flowing from the lubrication region into the porous material, yields a pressure field and thus effectively creates a force acting between the porous material and the surface, perpendicular to the surface. This force creates tangential friction between the porous material and the solid surface, thus preventing slip on the surface. Such a mechanism will allow for adhesion even in the absence of capillary forces and thus may explain how some frogs (such as river frogs) can maintain adhesion in the presence of rain or while being submerged (see Barnes *et al.* 2002; Endlein *et al.* 2013*b*). In addition, the time-varying nature of the suggested mechanism may explain why frogs periodically reposition their toes when connected to a surface (Endlein *et al.* 2013*a*,*b*).

The structure of this paper is as follows. In the next section, we illustrate the concept experimentally by a simplified configuration consisting of two surfaces connected by a liquid bridge and elastic springs. In § 3.1 we define the poroelastic problem. In § 3.2 we analyse the flow field and deformation field within the poroelastic medium. In § 3.3 we analyse the flow in the lubrication region between the toe pad and the solid surface, and in § 3.4 we obtain a governing equation for the dynamics of the toe pad, present several solutions and estimate viscous–poroelastic adhesion in frogs. In § 4 we summarize the results.

2. Experimental illustration of viscous–elastic friction creation

We initially focus on a simplified case in order to illustrate the effects of viscous–elastic interaction on friction. We examine the dynamics of two parallel surfaces connected by a liquid bridge and linearly elastic springs (see figure 1*a*). While in this case there are no poroelastic dynamics, it includes both viscous forces and elastic forces due to the liquid bridge and the linear springs, respectively. The springs are located outside of the liquid bridge and do not affect the flow field. Friction is created by the normal force applied by the springs on the contact area with the surface. The configuration is axisymmetric. We denote the gap between the two surfaces h, the viscosity μ, the surface tension γ, the density ρ, the liquid drop volume v_d, the liquid radius r_d, the total spring stiffness k, the relaxed spring length h_r (thus the normal force applied by the springs is $k(h-h_r)$) and the external normal force f_e (see figure 1*a*). Hereafter, characteristic values are denoted by asterisk superscripts. We define u^* as the characteristic speed, p^* as the characteristic pressure and h^* as the characteristic gap. Following Gat, Navaz & Gharib (2011), under the assumptions of a shallow liquid bridge ($h^*/r_d \ll 1$), negligible inertia of the liquid ($h^{*2}\rho u^*/\mu \ll 1$), negligible gravity ($g\rho h^*/p^* \ll 1$) and negligible capillary forces ($\gamma v_d/(h^*)^2 \ll 1$), the force balance equation is

$$f_e - \mu \frac{3v_d^2}{2\pi h^5}\frac{\mathrm{d}h}{\mathrm{d}t} + k(h_r - h) = 0. \tag{2.1}$$

The tangential friction acting at the solid interface is $f_t = \mu_s(h_r - h)k$, where μ_s is the friction coefficient. For cases in which both the springs and viscosity terms are

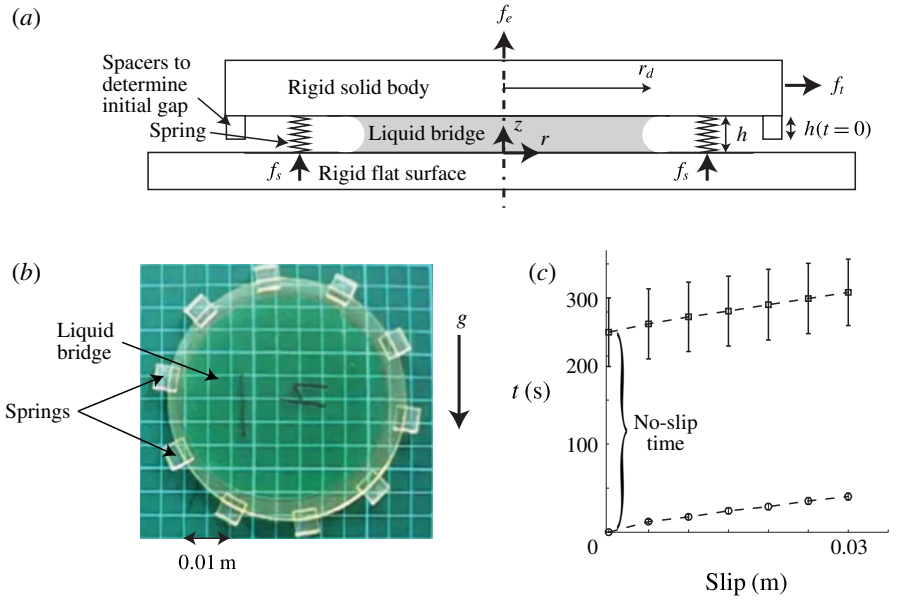

FIGURE 1. (Colour online) (*a*) An illustrative front view of the model. (*b*) An upper view photograph of the experimental model attached to a horizontal surface with a liquid bridge between. (*c*) Experimental results presenting time versus slip for plates with springs (squares) and without springs (circles). Bars present standard deviation.

non-negligible, an order-of-magnitude estimation yields the characteristic time scale $t^* = \mu v_d^2/\pi^2 k h^{*5}$. During this time scale, the springs will apply a normal force on the surface of the order of $\approx kh^*$, which will in turn create a tangential friction force.

We conducted experiments with a circular flat plate connected to 10 extended beams acting as linear elastic springs (see figure 1*b*). The solid was printed by an Objet Eden250 three-dimensional printer, and the material is Objet FullCure720. In all cases the configuration was tested immediately after printing and used only once. The liquid is a silicone oil droplet with volume $v_d = 5 \times 10^{-6}$ m^3, density $\rho = 750$ kg m^{-3}, surface tension 0.021 N m^{-1} and viscosity $\mu = 60$ Pa s. The plate was pressed against a rigid surface (positioned parallel to gravity; see figure 1*b*) and released at $t = 0$. The properties of the examined configuration are $k \approx 4.5 \times 10^4$ N m^{-1} and $h_r = 1.3$ mm. The order of magnitude of capillary forces is $2\gamma v_d/h^{*2} \approx 0.2$ N and is negligible compared with the order of magnitude of the elastic force $kh^* \approx 50$ N (where $h^* = 1$ mm). For such a configuration, the characteristic time scale is $t^* = \mu v_d^2/\pi^2 k h^{*5} = O(10^3$ s). We examined six identical plates and six control plates without springs. In all cases the initial gap was determined by spacers (see figure 1*a*) as $h(t = 0) = 0.8$ mm. The results are presented in figure 1(*c*) and clearly show enhancement of friction due to viscous–elastic interaction. While the control plates without springs immediately slipped, the configurations with springs slipped only at $\approx$250 s.

3. Adhesion due to viscous–poroelastic interaction

We now turn to analyse a more complex case of viscous–elastic interaction involving viscous flow within an elastic porous material as a mechanism to create adhesion.

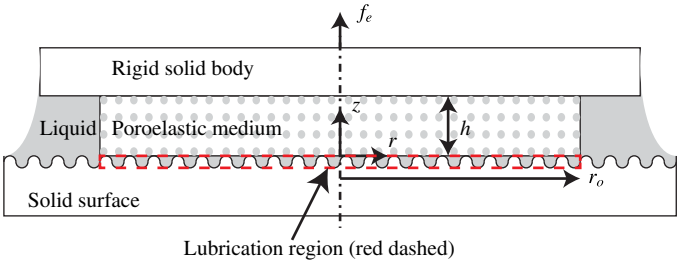

FIGURE 2. (Colour online) Illustrative description of the model consisting of a poroelastic material (dotted area) connecting a rigid body and a lubrication region (dashed; red online). The poroelastic material is axisymmetric with radius r_o, height h and external axial force f_e acting on the rigid body.

3.1. *Problem definition*

We model the interaction between an elastic porous material and a Newtonian fluid via the poroelastic mixture theory (Atkin & Craine 1976; Bowen 1980; Rajagopal & Tao 1995; Preziosi, Joseph & Beavers 1996). We focus on axisymmetric configurations with negligible inertial and capillary effects. The relevant regions are the poroelastic region and a thin liquid-filled gap between the poroelastic region and the rough surface (marked by the dashed line (red online) in figure 2). The relevant variables are the radius of the poroelastic material r_o, the poroelastic material height h, the poroelastic material relaxed height h_r (height when no stress is applied on the solid), the external force f_e, the solid fraction (i.e. ratio of solid volume to total volume of liquid and solid) Φ, the relaxed solid fraction Φ_r, the time t, the radial and axial coordinates $\boldsymbol{r} = (r, z)$, the solid velocity $\boldsymbol{v}_s = (u_s, v_s, w_s)$, the liquid velocity $\boldsymbol{v}_l = (u_l, v_l, w_l)$, the liquid viscosity μ, the solid density ρ_s, the liquid density ρ_l, the permeability $\boldsymbol{k}$ and the excess stress tensor $\boldsymbol{\sigma}$, defined as the stress tensor of the mixture minus the liquid pressure (see Preziosi *et al.* 1996).

3.2. *Analysis of the poroelastic medium*

The dynamics of a poroelastic medium saturated with a Newtonian incompressible liquid is governed by the conservation of mass of the solid,

$$\frac{\partial \Phi}{\partial t} + \boldsymbol{\nabla} \cdot (\Phi \boldsymbol{v}_s) = 0, \tag{3.1}$$

the conservation of mass of the liquid,

$$-\frac{\partial \Phi}{\partial t} + \boldsymbol{\nabla} \cdot [(1-\Phi)\boldsymbol{v}_l] = 0, \tag{3.2}$$

Darcy's law for the flow within the porous material,

$$\boldsymbol{v}_l - \boldsymbol{v}_s = -\frac{\boldsymbol{k}}{(1-\Phi)\mu}(\boldsymbol{\nabla} p - \rho_l \boldsymbol{g}), \tag{3.3}$$

and equation of the mixed momentum,

$$\rho_c \left(\frac{\partial \boldsymbol{v}_m}{\partial t} + \boldsymbol{v}_m \cdot \boldsymbol{\nabla} \boldsymbol{v}_m \right) = -\boldsymbol{\nabla} p + \boldsymbol{\nabla} \cdot \boldsymbol{\sigma} + [\rho_s \Phi + \rho_l (1-\Phi)]\boldsymbol{g}. \tag{3.4}$$

Here $\rho_c = \Phi\rho_s + (1-\Phi)\rho_l$ is the density of the mixture considered as a whole and $\boldsymbol{v}_m = [\Phi\rho_s\boldsymbol{v}_s + (1-\Phi)\rho_l\boldsymbol{v}_l]/\rho_c$ is the mass average velocity (see Preziosi *et al.* 1996).

The relevant boundary conditions are no solid velocity at $z=0$ and external velocity function $\boldsymbol{v}_e(t)$ at $z=h(t)$,

$$\boldsymbol{v}_s(z=0)=0, \quad \boldsymbol{v}_s(z=h(t))=\boldsymbol{v}_l(z=h(t))=\boldsymbol{v}_e(t). \tag{3.5a,b}$$

The initial conditions are

$$\Phi(t=0)=\Phi_i, \quad h(t=0)=h_i. \tag{3.6a,b}$$

Hereafter all normalized parameters are denoted by capital letters and characteristic values are denoted by asterisk superscripts. We define normalized coordinates R, Z and time T,

$$R=\frac{r}{r_o}, \quad Z=\frac{z}{h^*}, \quad T=\frac{t}{h^*/w^*}, \tag{3.7a–c}$$

normalized liquid velocity $\boldsymbol{V}_l$ and pressure P,

$$\boldsymbol{V}_l=\frac{\boldsymbol{v}_l}{w^*}, \quad P=\frac{p}{p^*}, \tag{3.8a,b}$$

normalized solid velocity $\boldsymbol{V}_s$, solid stress $\boldsymbol{\Sigma}$ and permeability $\boldsymbol{K}$,

$$\boldsymbol{V}_s=\frac{\boldsymbol{v}_s}{w^*}, \quad \boldsymbol{\Sigma}=\frac{\boldsymbol{\sigma}}{\boldsymbol{\sigma}^*}, \quad \boldsymbol{K}=\frac{\boldsymbol{k}}{k^*}, \tag{3.9a–c}$$

and poroelastic height H,

$$H=\frac{h(t)}{h^*}. \tag{3.10}$$

Here h^* is the characteristic height, w^* is the characteristic speed, p^* is the characteristic pressure, $\boldsymbol{\sigma}^*$ is the characteristic axial stress and k^* is the characteristic permeability.

Our analysis will focus on a thin geometry, defined as

$$\varepsilon_1=\frac{h^*}{r_o}\ll 1. \tag{3.11}$$

Substituting the normalized variables yields the leading-order form of (3.1)–(3.4) as

$$\frac{\partial\Phi}{\partial T}+\frac{\partial}{\partial Z}(\Phi W_s)+O(\varepsilon_1)=0, \tag{3.12}$$

$$-\frac{\partial\Phi}{\partial T}+\frac{\partial}{\partial Z}[(1-\Phi)W_l]+O(\varepsilon_1)=0, \tag{3.13}$$

$$W_l - W_s = -\frac{k^* p^*}{\mu w^* h^*}\frac{K_{zz}}{(1-\Phi)}\frac{\partial P}{\partial Z} + O\left(\varepsilon_1, \frac{\rho_l g k_0}{\mu w^*}\right) \tag{3.14}$$

and

$$\frac{\partial P}{\partial Z} = \frac{\sigma^*}{p^*}\frac{\partial \Sigma_{zz}}{\partial Z} + O\left(\varepsilon_1, \frac{\rho_j (w^*)^2}{p^*}, \frac{[\rho_s \Phi + \rho_l(1-\Phi)]g}{p^*}\right), \tag{3.15}$$

where Σ_{zz} and K_{zz} are the axial terms of $\boldsymbol{\Sigma}$ and $\boldsymbol{K}$, respectively, and W_s and W_l are the axial solid and liquid speeds, respectively.

Following the previous works of Anderson (2005), Siddique (2009) and Siddique, Anderson & Bondarev (2009), the constitutive relationships for the permeability k and stress σ are approximated as

$$k_{zz} = \frac{k_0}{\Phi}, \quad \sigma = m(\Phi_r - \Phi), \tag{3.16a,b}$$

where $k_0 > 0$ and $m > 0$ are known constants defining the poroelastic material permeability and stiffness, respectively. Order of magnitude analysis of (3.15) and (3.16) yield $p^* = \sigma^* = m$ and $k^* = k_0$.

We define the scaled coordinate $\Psi = z/h(t)$ and formulate the problem according to Preziosi *et al.* (1996). Adding (3.13) and (3.12), integrating over Z and using (3.5) we obtain

$$W_l(1-\Phi) + \Phi W_s = \frac{\partial H}{\partial T}. \tag{3.17}$$

From (3.14) and (3.17),

$$W_s = \frac{\partial H}{\partial T} - \frac{mk_0}{\mu w^* h^*}\frac{1}{\Phi H(T)}\frac{\partial \Phi}{\partial \Psi} \tag{3.18}$$

and

$$W_l = \frac{\partial H}{\partial T} + \frac{mk_0}{\mu w^* h^*}\frac{1}{(1-\Phi)H(T)}\frac{\partial \Phi}{\partial \Psi}. \tag{3.19}$$

Combining (3.19) and (3.12) together with (3.15) yields

$$\frac{\partial \Phi}{\partial T} + (1-\Psi)\frac{\partial H}{\partial T}\frac{1}{H(T)}\frac{\partial \Phi}{\partial \Psi} = \frac{mk_0}{\mu w^* h^*}\frac{1}{H^2(T)}\frac{\partial^2 \Phi}{\partial \Psi^2}. \tag{3.20}$$

We express the boundary conditions (3.5) in terms of solid fraction Φ as

$$\frac{mk_0}{\mu w^* h^*}\frac{\partial \Phi}{\partial \Psi} = 0, \quad \Psi = 1, \tag{3.21}$$

and

$$\frac{mk_0}{\mu w^* h^*}\frac{\partial \Phi}{\partial \Psi} - H(T)\frac{\partial H}{\partial T}\Phi = 0, \quad \Psi = 0, \tag{3.22}$$

where $\mu w^* h^*/mk_0$ can be interpreted as the ratio between the characteristic speed of the poroelastic problem, w^*, and the characteristic speed of the viscous flow, $mk_0/\mu h^*$.

3.3. *Analysis of lubrication region*

We denote by tildes the liquid velocity $\tilde{\boldsymbol{v}}_l = (\tilde{u}_l, \tilde{w}_l)$ in the lubrication region, where $\tilde{u}_l$ is the radial speed and $\tilde{w}_l$ is the axial speed. The governing equations in the lubrication region are the axisymmetric Stokes equations for Newtonian incompressible liquid,

$$\boldsymbol{\nabla} p = \mu \nabla^2 \tilde{\boldsymbol{v}}_l, \tag{3.23}$$

and conservation of mass,

$$\boldsymbol{\nabla} \cdot \tilde{\boldsymbol{v}}_l = 0. \tag{3.24}$$

The relevant boundary conditions are gauge pressure $p = 0$ at $r = r_o$, symmetry $\partial p/\partial r = 0$ at $r = 0$, no-slip and no-penetration $\tilde{\boldsymbol{v}}_l = 0$ at the solid interface and mass-flux and pressure matching to the poroelastic region $\tilde{w}_l = (1 - \Phi) w_l$ at $z = 0$. The liquid slip at the boundary of the porous material, $z = 0$, is proportional to $\sqrt{k_0}\, \partial \tilde{u}_l/\partial z$, where $\sqrt{k_0}$ is the characteristic length scale of the permeable material (Beavers & Joseph 1967). We relate the characteristic roughness $\tilde{h}$ to average viscous resistance by defining

$$\tilde{h}^{-3} = \frac{1}{A} \int_A h_s^{-3} \, \mathrm{d}A, \tag{3.25}$$

where h_s is the local gap between the solid surface and the poroelastic surface and A is a sufficiently large surface area on the z plane. The normalized velocity $\tilde{U}_l$, $\tilde{W}_l$ and $\tilde{Z}$ coordinate for the lubrication region are defined as

$$\tilde{U}_l = \frac{u}{u^*}, \quad \tilde{W}_l = \frac{\tilde{W}_l}{w^*}, \quad \tilde{Z} = \frac{z}{\tilde{h}}. \tag{3.26a–c}$$

We require sufficiently small k_0 so that

$$\varepsilon_2 = \frac{k_0 h^*}{\tilde{h}^3/12} \ll 1, \quad \varepsilon_3 = \frac{u_l(Z=0)}{u^*} = \frac{\sqrt{k_0}}{h^*} \ll 1, \tag{3.27a,b}$$

representing the scaled pore size and the slip at the boundary of the poroelastic surface. For $\varepsilon_3 \ll 1$ we require $\tilde{U}_l = 0$ at $\tilde{Z} = 0$. (The lubrication region may also be modelled as a porous region of depth h_p and radial permeability k_p, where $\tilde{h}^3/12 = k_p h_p$.)

Substituting (3.26) into (3.23) and (3.24), an order-of-magnitude analysis yields

$$u^* = \frac{w^* r_o}{\tilde{h}}, \quad w^* = \frac{m\tilde{h}^3/12}{\mu r_0^2}, \tag{3.28}$$

and normalized equation (3.23) is thus

$$\frac{\partial P}{\partial R} \sim \frac{1}{H_s^3} \int_{-H_s}^{0} \tilde{U}_l \, \mathrm{d}\tilde{Z}, \quad \frac{\partial P}{\partial \tilde{Z}} \sim 0, \tag{3.29a,b}$$

where $H_s = h_s/\tilde{h}$ is the local normalized gap. We substitute (3.29) into (3.24) and apply the boundary conditions $\tilde{W}_l = (1 - \Phi) W_l$ at $\tilde{Z} = 0$ (flux matching between the lubrication region and the poroelastic region) and $\tilde{U}_l = \tilde{W}_l = 0$ at the solid surface. Thus we obtain the pressure distribution in the lubrication region. Substituting into the variables of the poroelastic region and utilizing (3.25) yields

$$P(\Psi = 0) \sim -(1 - \Phi(\Psi = 0)) W_l(\Psi = 0) \frac{1 - R^2}{4}. \tag{3.30}$$

3.4. *Results*

3.4.1. *Governing equations*

Substituting (3.28) into (3.20)–(3.22) yields

$$\frac{mk_0}{\mu w^* h^*} = \frac{k_0 h^*}{\tilde{h}^3/12}\frac{r_o^2}{(h^*)^2} = \frac{\varepsilon_2}{\varepsilon_1^2} \tag{3.31}$$

and the governing equation

$$\frac{1}{H^2}\frac{\partial^2 \Phi}{\partial \Psi^2} - \frac{\varepsilon_1^2}{\varepsilon_2}\left[\frac{\partial \Phi}{\partial T} + (1-\Psi)\frac{\partial H}{\partial T}\frac{1}{H}\frac{\partial \Phi}{\partial \Psi}\right] = 0, \tag{3.32}$$

with the boundary conditions

$$\frac{\partial \Phi}{\partial \Psi} - \frac{\varepsilon_1^2}{\varepsilon_2} H \frac{\partial H}{\partial T}\Phi = 0, \quad \Psi = 0, \tag{3.33}$$

$$\frac{\partial \Phi}{\partial \Psi} = 0, \quad \Psi = 1, \tag{3.34}$$

and the initial condition

$$\Phi = \Phi_i, \quad T = 0. \tag{3.35}$$

The liquid speed W_l and solid speed W_s are thus

$$W_s = \frac{\partial H}{\partial T} - \frac{\varepsilon_2}{\varepsilon_1^2}\frac{1}{\Phi H(T)}\frac{\partial \Phi}{\partial \Psi}, \quad W_l = \frac{\partial H}{\partial T} + \frac{\varepsilon_2}{\varepsilon_1^2}\frac{1}{(1-\Phi)H(T)}\frac{\partial \Phi}{\partial \Psi}. \tag{3.36a,b}$$

Substituting (3.36) into (3.30) yields the gauge pressure at $Z = 0$:

$$P(Z=0) = -(1-\Phi(0))\left(\frac{\partial H}{\partial T} + \frac{\varepsilon_2}{\varepsilon_1^2}\frac{1}{(1-\Phi(0))H}\frac{\partial \Phi(0)}{\partial \Psi}\right)\frac{1-R^2}{4}. \tag{3.37}$$

Integration over $P(Z=0)$ will yield the total normal force applied by the liquid. The external force applied on the poroelastic material $F_e = f_e/mr_o^2$ (see figure 2) is balanced by the force applied by the solid surface (denoted hereafter as $F_s = \pi(\Phi_r - \Phi(\Psi = 0))$ and normalized by mr_o^2) and the force applied by the liquid gauge pressure at $\Psi = 0$. The force balance equation, $F_e = \int_0^1 (\Sigma_{zz} - P)2\pi R\,\mathrm{d}R$, yields the expression for the external force:

$$F_e = \pi(\Phi_r - \Phi(\Psi=0)) + \frac{\pi}{8}(1-\Phi(0))\left(\frac{\partial H}{\partial T} + \frac{\varepsilon_2}{\varepsilon_1^2}\frac{1}{(1-\Phi(0))H}\frac{\partial \Phi(0)}{\partial \Psi}\right). \tag{3.38}$$

For the limit $\varepsilon_1^2/\varepsilon_2 \ll 1$ we define the asymptotic expansion

$$\Phi = \Phi_0 + \left(\frac{\varepsilon_1^2}{\varepsilon_2}\right)\Phi_1 + \left(\frac{\varepsilon_1^2}{\varepsilon_2}\right)^2 \Phi_2 + O\left[\left(\frac{\varepsilon_1^2}{\varepsilon_2}\right)^3\right]. \tag{3.39}$$

(We focus on the limit $\varepsilon_1^2/\varepsilon_2 \ll 1$ since it agrees with the characteristic physical parameters of frogs' toe pads; see § 3.4.4.) We substitute (3.39) into (3.32)–(3.35).

The leading-order problem yields that $\Phi_0(T)$ is a function of time only. The first-order terms of (3.32) and (3.34) yield

$$\Phi_1 = H^2 \frac{\partial \Phi_0}{\partial T}\left(\frac{\Psi^2}{2} - \Psi\right) + C_1(T). \tag{3.40}$$

Substituting Φ_0 and Φ_1 into the order $O(\varepsilon_1^2/\varepsilon_2)$ boundary condition at $\Psi = 0$, equation (3.33) yields an ordinary differential equation with respect to time:

$$\frac{\partial \Phi_0}{\partial T} + \frac{\partial H}{\partial T}\frac{\Phi_0}{H} = 0. \tag{3.41}$$

Solving (3.41) with (3.35) yields $\Phi_0 = \Phi_i H(0)/H(T)$. We determine $C_1(T)$ from the order $O[(\varepsilon_1^2/\varepsilon_2)^2]$ equation (3.32),

$$\frac{\partial^2 \Phi_2}{\partial \Psi^2} = H^2 \frac{\partial \Phi_1}{\partial T} + (1-\Psi)\frac{\partial H}{\partial T} H \frac{\partial \Phi_1}{\partial \Psi}, \tag{3.42}$$

and the $O[(\varepsilon_1^2/\varepsilon_2)^2]$ boundary and initial conditions. Substituting (3.40) into (3.42) and applying (3.34), we obtain an ordinary differential equation from the boundary condition at $\Psi = 0$, similarly to (3.41), for the order $O(\varepsilon_1^2/\varepsilon_2)$:

$$\frac{\partial C_1}{\partial T} + \frac{\partial H}{\partial T}\frac{1}{H} C_1 = -\frac{1}{3}\frac{\Phi_i H(0)}{H}\frac{\partial}{\partial T}\left(H\frac{\partial H}{\partial T}\right). \tag{3.43}$$

Applying (3.35) we solve (3.43) and obtain

$$C_1 = -\frac{H(0)}{3}\Phi_i \frac{\partial H}{\partial T}. \tag{3.44}$$

Thus Φ to order $O(\varepsilon_1^2/\varepsilon_2)$ is

$$\frac{\Phi}{\Phi_i} \sim \frac{H(0)}{H} + \frac{\varepsilon_1^2}{\varepsilon_2} H(0)\frac{\partial H}{\partial T}\left(\Psi - \frac{\Psi^2}{2} - \frac{1}{3}\right), \tag{3.45}$$

and from (3.35) we obtain the requirement $\partial H(0)/\partial T = 0$ in order to satisfy the spatially uniform initial condition.

3.4.2. *Externally controlled H for* $\varepsilon_1^2/\varepsilon_2 \ll 1$

Based on (3.45) and (3.38) we can calculate F_e required to achieve an arbitrary $H(T)$. After calculating $H(T)$, exact solutions of the solid fraction Φ, fluid velocity W_l, solid velocity W_s and internal stress Σ can be obtained from (3.45) and (3.36)–(3.38). Figure 3 presents the case of $\partial H/\partial T = \tanh(CT)$, where $C = 100$, and thus $\partial H/\partial T \approx 1$ for $T > 0.02$. The initial uniform solid fraction of the poroelastic medium is $\Phi_i = 0.6$, relaxed solid fraction is $\Phi_r = 0.4$, and $\varepsilon_1^2/\varepsilon_2 = 0.1$. Panel (*a*) presents the change in poroelastic layer height $H - 1$ (dash-dotted), external force F_e (solid), total force by the liquid pressure F_p (dashed) and force applied by the solid surface F_s (dotted). The total force by the liquid pressure F_p becomes nearly constant from $T \approx 0.03$ (as $\partial H/\partial T \to 1$), while F_s decreases in time. The external force is initially negative

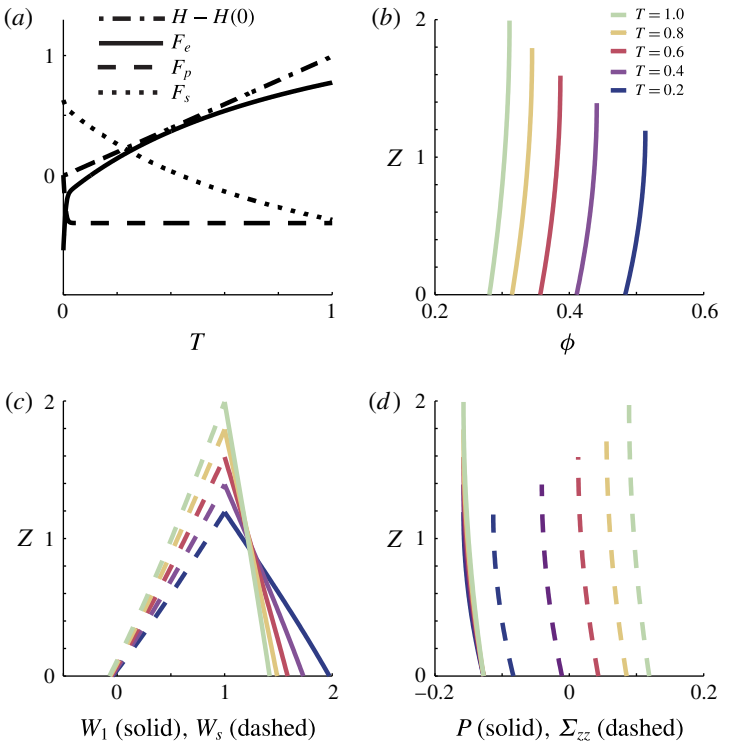

FIGURE 3. (Colour online) Configuration with speed $\partial H/\partial T = \tanh(100T)$ (effectively $\partial H/\partial T \approx 1$ for $T > 0.02$). The initial uniform solid fraction of the poroelastic medium is $\Phi_i = 0.6$, relaxed solid fraction is $\Phi_r = 0.4$ and $\varepsilon_1^2/\varepsilon_2 = 0.1$. (*a*) Change in gap $H - 1$ (dash-dotted), external required force F_e (solid), total force by the liquid pressure F_p (dashed) and force applied by the solid surface F_s (dotted); (*b*) solid fraction Φ, (*c*) liquid speed W_l (solid) and solid speed W_s (dashed) and (*d*) pressure P (solid) and axial stress Σ_{zz} versus Z for various normalized times $T = 0.2$, 0.4, 0.6, 0.8 and 1 (blue, purple, red, yellow and green online, respectively).

and prevents the compressed poroelastic material from expanding more rapidly than the required $\partial H/\partial T = 1$. From $T \approx 0.1$, F_e is positive and acts to increase $\partial H/\partial T$. In panels (*b–d*) the various curves (blue, purple, red, yellow and green online) mark normalized time $T = 0.2$, 0.4, 0.6, 0.8 and 1, respectively. Panel (*b*) presents solid fraction Φ versus Z for various times, showing the decrease of Φ with time and as $Z \to 0$. Panel (*c*) presents liquid speed W_l (solid) and solid speed W_s (dashed) versus Z for various times. Both speeds are approximately linear with Z with gradients decreasing with time. Panel (*d*) presents pressure P (solid) and axial stress Σ_{zz} (dashed) versus Z for various times. The average pressure P is approximately constant, owing to the uniform liquid mass flux into the poroelastic material. The axial stress increases with time because of the forced deformation of the poroelastic material. Owing to the initial compression, the axial stress is negative until $T \approx 0.4$ and then becomes positive as a result of stretching by the external force.

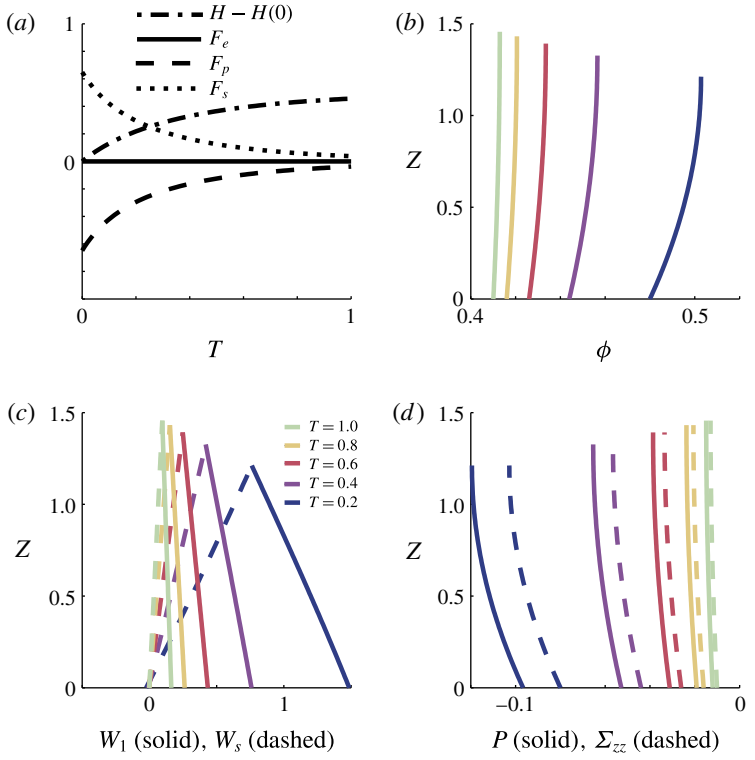

FIGURE 4. (Colour online) Configuration with initial compression and a sudden release at $T=0$ with $F_e=0$. The initial uniform solid fraction of the poroelastic medium is $\Phi_i=0.6$, relaxed solid fraction is $\Phi_r=0.4$ and $\varepsilon_1^2/\varepsilon_2=0.1$. (*a*) Change in poroelastic layer height $H-1$ (dash-dotted), external required force F_e (solid), total force by the liquid pressure F_p (dashed) and force applied by the solid surface F_s (dotted); (*b*) solid fraction Φ, (*c*) liquid speed W_l (solid) and solid speed W_s (dashed) and (*d*) pressure P (solid) and stress Σ_{zz} versus Z for various normalized times $T=0.2$, 0.4, 0.6, 0.8 and 1 (blue, purple, red, yellow and green online, respectively).

3.4.3. *Externally controlled F_e for $\varepsilon_1^2/\varepsilon_2 \ll 1$*

We apply (3.45) with (3.38) to obtain H as a function of the external force acting on the poroelastic material for $\varepsilon_1^2/\varepsilon_2 \ll 1$,

$$F_e = \pi\left(\Phi_r - \Phi_i\frac{H(0)}{H}\right) + \frac{\pi}{8}\frac{\partial H}{\partial T}. \tag{3.46}$$

For constant F_e, separation of variables yields an implicit solution of $H(T)$,

$$T = \frac{\pi}{8}\left[\frac{H-H(0)}{F_e-\pi\Phi_r} - \frac{\pi\Phi_i H(0)}{(F_e-\pi\Phi_r)^2}\ln\left(\frac{H(F_e-\pi\Phi_r)-\pi\Phi_i H(0)}{H(0)(F_e-\pi\Phi_r)-\pi\Phi_i H(0)}\right)\right]. \tag{3.47}$$

Figure 4 presents the case of initial compression of the poroelastic material, with sudden release $F_e=0$, solved by (3.47). For $F_e=0$, exact solutions of the solid fraction Φ, fluid velocity W_l, solid velocity W_s and internal stress Σ_{zz} are calculated from (3.45) and (3.36)–(3.38). The initial uniform solid fraction of the poroelastic

medium is $\Phi_i = 0.6$, relaxed solid fraction is $\Phi_r = 0.4$, initial height is $H(0) = 1$ and $\varepsilon_1^2/\varepsilon_2 = 0.1$. Panel (*a*) presents the change in poroelastic layer height $H - 1$ (dash-dotted), external required force F_e (solid), total force by the liquid pressure F_p (dashed) and force applied by the solid surface F_s (dotted). The absolute value of the force applied by the liquid pressure F_p decreases while the sign of F_p is negative for all T. The force applied by the solid surface F_s decreases in time and is positive for all T. The speed $\partial H/\partial T$ is maximal at $T = 0$ and decreases with time as the configuration reaches a steady balance. In panels (*b–d*) the various curves (blue, purple, red, yellow and green online) mark normalized time $T = 0.2$, 0.4, 0.6, 0.8 and 1, respectively. Panel (*b*) presents solid fraction Φ versus Z for various times, showing a decrease of Φ with time and nearly constant values with Z. Panel (*c*) presents liquid speed W_l (solid) and solid speed W_s (dashed) versus Z for various times. Both speeds are approximately linear with Z with gradients decreasing with time. Panel (*d*) presents pressure P (solid) and axial stress Σ_{zz} (dashed) versus Z for various times. Since no external forces act on the system, the dominant balance is between pressure P and axial stress and thus $P \approx \Sigma_{zz}$. The magnitude of both parameters decreases with time as the system approaches steady balance.

3.4.4. *Characteristic values of frogs' toe pads and adhesion time estimation*

We estimate, based on existing works, the order of magnitude of the relevant physical properties of frogs' toe pads. We focus on torrent frogs because of their ability to keep adhesion underwater and thus without capillary forces. Based on Federle *et al.* (2006) and Endlein *et al.* (2013*a*), we obtain that the total toe pad area is 10^{-4} m^2, the number of toes is 18, yielding individual toe pad radius of $r_o = 1.3 \times 10^{-3}$ m (assuming circular toe pads), the frog mass is 2.7×10^{-3} kg, the viscosity of the mucus is $\mu \approx 10^{-3}$ Pa s, the toe pad height is $h_r = 10^{-5}$ m, and the permeability of the frogs' toe pad is calculated via $k_0 \approx d_p^2/4$, where $d_p = 10^{-7}$ m is the characteristic length scale of the pores. We examine various values of the characteristic gap in the lubrication region $\tilde{h}$ and the stiffness parameter m. For $\tilde{h} = 10^{-6}$ m, we obtain $\varepsilon_1 = h^*/r_o \approx 6.3 \times 10^{-3}$ and $\varepsilon_2 = k_0 h^*/12\tilde{h}^3 = 0.1$, thus $\varepsilon_1^2/\varepsilon_2 \approx 4 \times 10^{-4}$.

Slip will occur when $f_t \geqslant f_s \mu_s$, where f_s is the dimensional normal force acting on the surface, μ_s is the friction coefficient and f_t is a tangential force (see figure 5*a*). Utilizing $F_s = \pi(\Phi_r - \Phi(\Psi = 0))$, we can obtain Φ_s, the solid fraction at $\Psi = 0$ for which slip will occur,

$$\Phi_s = \Phi_r - \frac{1}{\mu_s} \frac{f_t}{m\pi r_o^2}. \tag{3.48}$$

Substituting (3.45) into (3.48) yields H_s, the height of the poroelastic medium when slip occurs,

$$H_s = \frac{\Phi_i}{\Phi_s}, \tag{3.49}$$

and substituting (3.49) into (3.47) yields the adhesion time t_a.

Figure 5 presents the dimensional adhesion time t_a for various configurations and parameters. Panel (*a*) presents the slope angle θ and the normal forces. The normal force is $f_e = -\cos(\theta) m_f g/n_t$ and the tangential force is $f_t = |\sin(\theta) m_f g/n_t|$, where m_f is the mass of the frog, g is gravity and n_t is the number of frog toes. Panels (*b–c*) present the adhesion time t_a for different frog masses of 10^{-3} kg (dashed), 2×10^{-3} kg (dashed) and 3×10^{-3} kg (dotted) at $\theta = 60°$. Panel (*b*) presents the adhesion time t_a versus stiffness parameter m for $\Phi_i = 0.85$ and $\theta = 60°$. For stiffness

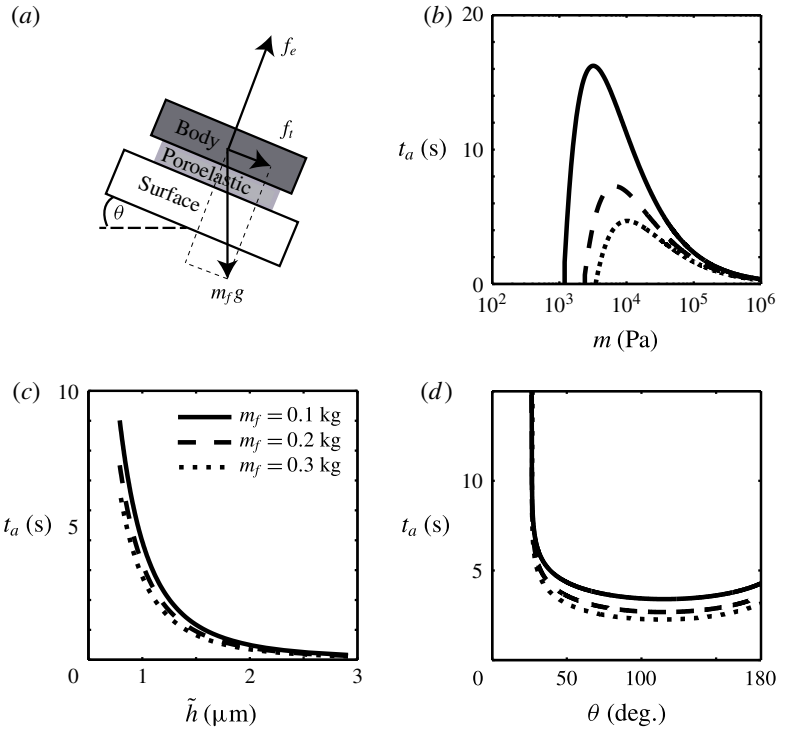

FIGURE 5. Adhesion time (time until tangential slip occurs) t_a for various physical parameters: (a) the slope angle θ and the normal f_e and tangential f_t forces: (b) adhesion time t_a versus the stiffness of the poroelastic material m for $\theta = 60^\circ$ and $\Phi_i = 0.85$; (c) adhesion time t_a versus the initial solid fraction Φ_i (initial compression) for $\theta = 60^\circ$ and $m = 5 \times 10^5$ (Pa); (d) adhesion time t_a versus slope angle θ for $\Phi_i = 0.85$ and $m = 5 \times 10^5$ (Pa). Frog masses of 10^{-3} kg (solid), 2×10^{-3} kg (dashed) and 3×10^{-3} kg (dotted) are presented. In all cases $\Phi_r = 0.7$.

parameter below a critical value ($m \approx 10^3$ Pa), no adhesion is created. With increasing m, a maximum of adhesion time is presented, as well as a monotonic decrease in adhesion time as $m \to \infty$. Panel (c) presents the adhesion time t_a versus characteristic gap in the lubrication region $\tilde{h}$ (defined by (3.25)), for $\theta = 60^\circ$ and $m = 5 \times 10^5$ Pa. A monotonic increase in adhesion time with decreasing $\tilde{h}$ is observed. Panel (d) presents the adhesion time versus slope angle θ for $\Phi_i = 0.85$ and $m = 5 \times 10^5$ Pa. Below a critical minimal value of θ, steady adhesion is achieved. With increasing θ, there is a decrease in the adhesion time until a minimum value, and then a moderate maximum at $\theta = 180^\circ$. In all cases we observe a monotonic increase in adhesion time with reduction of frog mass.

4. Concluding remarks

In this work, we have suggested viscous–elastic interaction as being a mechanism to explain the adhesion of frogs' toe pads. We applied a poroelastic model for the toe pad and a lubrication approximation for the flow between the toe pad and the solid surface. We obtained a governing equation for the solid fraction, which can be solved and then applied to obtain the solid stress, solid velocity, liquid pressure

and liquid velocity. The viscous–elastic interaction was shown to be able to create temporary adhesion, even in the absence of capillary forces, and the adhesion time was estimated for physical parameters chosen from an order-of-magnitude estimation of frogs' toe pads. A maximum for the adhesion time was observed with regard to m, the stiffness parameter of the poroelastic medium, and a minimum with regard to the slope angle of the surface. The time-dependent nature of viscous–elastic adhesion is in agreement with the periodic repositioning of frogs' toe pads during adhesion to surfaces. This analysis focused on a single toe pad; however, the dynamics of a complete frog includes multiple toe pads, which are repositioned at different times. Thus the computed adhesion time t_a representing the time a single toe pad is connected to a surface may differ significantly from the adhesion time of the entire frog.

Acknowledgement

This research was supported by the Israel Science Foundation (grant 818/13).

Appendix A. Dimensional equations and boundary conditions

The dimensional governing equation for Φ, the solid fraction, is

$$\frac{\partial \Phi}{\partial t} + \frac{\partial}{\partial z}\left[\Phi\left(\frac{\partial h}{\partial t} - \frac{mk_0}{\mu}\frac{\partial \Phi}{\partial z}\right)\right] = 0, \tag{A 1}$$

with the dimensional boundary conditions

$$\frac{\partial \Phi}{\partial z} - \frac{\mu}{mk_0}\frac{\partial h}{\partial t}\Phi = 0, \quad z = 0, \tag{A 2}$$

$$\frac{\partial \Phi}{\partial z} = 0, \quad z = h(t), \tag{A 3}$$

and the initial condition

$$\Phi = \Phi_i, \quad t = 0. \tag{A 4}$$

Here the parameters k_0, m and Φ_r representing permeability, stiffness parameter and relaxed solid fraction, respectively, are known constants defining the properties of the poroelastic medium by the relations (following Anderson 2005; Siddique 2009; Siddique *et al.* 2009)

$$k_{zz} = \frac{k_0}{\Phi}, \quad \sigma = m(\Phi_r - \Phi). \tag{A 5a,b}$$

The dimensional liquid speed w_l and solid speed w_s are

$$w_s = \frac{\partial h}{\partial t} - \frac{mk_0}{\mu(1-\Phi)}\frac{\partial \Phi}{\partial z} \tag{A 6}$$

and

$$w_l = \frac{\partial h}{\partial t} + \frac{mk_0}{\mu\Phi}\frac{\partial \Phi}{\partial z}. \tag{A 7}$$

The dimensional gauge pressure at $z = 0$ is

$$p(z=0) = -3\frac{\mu r_o^2}{\tilde{h}^3}(1-\Phi(0))\left(\frac{\partial h}{\partial t} + \frac{mk_0}{\mu(1-\Phi(0))}\frac{\partial \Phi(0)}{\partial z}\right)\left(1 - \frac{r^2}{r_o^2}\right). \tag{A 8}$$

The dimensional force balance equation of the poroelastic medium is

$$f_e = \frac{3\pi}{2}\frac{\mu r_o^2}{\tilde{h}^3}(1-\Phi(0))\left(\frac{\partial h}{\partial t}+\frac{mk_0}{\mu(1-\Phi(0))}\frac{\partial \Phi(0)}{\partial z}\right) - m\pi r_o^2(\Phi(z=0)-\Phi_r), \quad \text{(A 9)}$$

where f_e is the external force. Slip occurs when $f_t > \mu_s f_s$, where f_s given by $f_s = m\pi r_o^2(\Phi(z=0)-\Phi_r)$ is the normal force applied by the solid fraction of the poroelastic material and μ_s is the friction coefficient.

For $\varepsilon_1^2/\varepsilon_2 \to 0$ we obtain the relation between Φ and h as

$$\frac{\Phi}{\Phi_i} \sim \frac{h(0)}{h} + \frac{\mu h(0)}{mk_0}\frac{\partial h}{\partial t}\left(\frac{z}{h}-\frac{1}{2}\frac{z^2}{h^2}-\frac{1}{3}\right). \quad \text{(A 10)}$$

REFERENCES

AMBROSI, D. & PREZIOSI, L. 2000 Modeling injection molding processes with deformable porous preforms. *SIAM J. Appl. Maths* **61** (1), 22–42.

ANDERSON, D. 2005 Imbibition of a liquid droplet on a deformable porous substrate. *Phys. Fluids* **17** (8), 087104.

ATKIN, R. & CRAINE, R. 1976 Continuum theories of mixtures: basic theory and historical development. *Q. J. Mech. Appl. Maths* **29** (2), 209–244.

BARNES, J., SMITH, J., OINES, C. & MUNDL, R. 2002 Bionics and wet grip. *Tire Technol. Intl* **2002** (December), 56–60.

BATTIATO, I. 2012 Self-similarity in coupled Brinkman/Navier–Stokes flows. *J. Fluid Mech.* **699**, 94–114.

BATTIATO, I., BANDARU, P. R. & TARTAKOVSKY, D. M. 2010 Elastic response of carbon nanotube forests to aerodynamic stresses. *Phys. Rev. Lett.* **105** (14), 144504.

BEAVERS, G. & JOSEPH, D. 1967 Boundary conditions at a naturally permeable wall. *J. Fluid Mech.* **30**, 197–207.

BIOT, M. 1972 Theory of finite deformations of porous solids. *Indiana Univ. Math. J.* **21** (7), 597–620.

BOWEN, R. 1980 Incompressible porous media models by use of the theory of mixtures. *Intl J. Engng Sci.* **18** (9), 1129–1148.

EMERSON, S. & DIEHL, D. 1980 Toe pad morphology and mechanisms of sticking in frogs. *Biol. J. Linnean Soc.* **13** (3), 199–216.

ENDLEIN, T., BARNES, W. J. P., SAMUEL, D. S., CRAWFORD, N. A., BIAW, A. B. & GRAFE, U. 2013*a* Sticking under wet conditions: the remarkable attachment abilities of the torrent frog, *Staurois guttatus*. *PLoS ONE* **8** (9), e73810.

ENDLEIN, T., JI, A., SAMUEL, D., YAO, N., WANG, Z., BARNES, W. J. P., FEDERLE, W., KAPPL, M. & DAI, Z. 2013*b* Sticking like sticky tape: tree frogs use friction forces to enhance attachment on overhanging surfaces. *J. R. Soc. Interface* **10** (80), 20120838.

ERNST, V. 1973*a* The digital pads of the tree frog, *Hyla cinerea*. I. The epidermis. *Tissue Cell* **5** (1), 83–96.

ERNST, V. 1973*b* The digital pads of the tree frog, *Hyla cinerea*. II. The mucous glands. *Tissue Cell* **5** (1), 97–104.

FEDERLE, W. 2006 Why are so many adhesive pads hairy? *J. Expl Biol.* **209** (14), 2611–2621.

FEDERLE, W., BARNES, W., BAUMGARTNER, W., DRECHSLER, P. & SMITH, J. 2006 Wet but not slippery: boundary friction in tree frog adhesive toe pads. *J. R. Soc. Interface* **3** (10), 689–697.

GAT, A., NAVAZ, H. & GHARIB, M. 2011 Dynamics of freely moving plates connected by a shallow liquid bridge. *Phys. Fluids* **23** (9), 097101.

GREEN, D. 1979 Treefrog toe pads: comparative surface morphology using scanning electron microscopy. *Can. J. Zool.* **57** (10), 2033–2046.

HANNA, G., JON, W. & BARNES, W. 1991 Adhesion and detachment of the toe pads of tree frogs. *J. Expl Biol.* **155** (1), 103–125.

PERSSON, B. 2007 Wet adhesion with application to tree frog adhesive toe pads and tires. *J. Phys.: Condens. Matter* **19** (37), 376110.

PREZIOSI, L., JOSEPH, D. & BEAVERS, G. 1996 Infiltration of initially dry, deformable porous media. *Intl J. Multiphase Flow* **22** (6), 1205–1222.

RAJAGOPAL, K. & TAO, L. 1995 *Mechanics of Mixtures*. World Scientific.

SIDDIQUE, J. 2009 Newtonian and non-Newtonian flows into deformable porous materials. PhD thesis, George Mason University, Fairfax, VA.

SIDDIQUE, J., ANDERSON, D. & BONDAREV, A. 2009 Capillary rise of a liquid into a deformable porous material. *Phys. Fluids* **21** (1), 013106.

TSIPENYUK, A. & VARENBERG, M. 2014 Use of biomimetic hexagonal surface texture in friction against lubricated skin. *J. R. Soc. Interface* **11**, 20140113.